Development of a Fast-Response Calorimeter Heat Transfer Gauge for Hypersonic Ground Testing

Rowland T. Penty Geraets* Matthew McGilvray † and Luke J. Doherty ‡
University of Oxford, Oxford, U.K.

Richard G. Morgan§ and Christopher M. James¶ and Tristan Vanyai‖
University of Queensland, Brisbane, Australia

David R. Buttsworth**
University of Southern Queensland, Toowoomba, Australia

A robust, fast response calorimeter based heat transfer gauge called the Diamond Heat Transfer Gauge (DHTG) has been developed for use in transient hypersonic ground test facilities. Desirable response time and robustness are achieved by using a 75 µm to 300 µm thick layer of synthetic diamond as the calorimeter and a platinum thin film resistance thermometer to measure the temperature rise. Different versions of the gauge have been shown experimentally to have a rise time of between 7 µs and 28 µs. The gauges have measured peak heat fluxes up to 300 MW/m² in flows with total enthalpies of 50 MJ/kg over multiple shots in the X2 expansion tunnel at the University of Queensland. Experimentally measured heat fluxes have been shown to compare well with surface junction thermocouples and thin film heat transfer gauges.

Nomenclature

AOA	Angle Of Attack
CVD	Chemical Vapour Deposition
$DHTG$	Diamond Heat Transfer Gauge
PCD	Polycrystalline Diamond
SCD	Single Crystal Diamond
TC	Thermocouple
α	Thermal diffusivity
α_R	Coefficient of Temperature with resistance
a	Ratio of thermal products
c	Specific heat capacity
e	Thermal effusivity
I_0	Thin film current supply
l	Calorimeter thickness
q	Heat flux
R_0	Resistance at 0 °C

*DPhil Candidate, Department of Engineering Science, The University of Oxford
†Associate Professor, Department of Engineering Science, The University of Oxford
‡Post-Doctoral Research Assistant, Department of Engineering Science, The University of Oxford
§Professor, Centre for Hypersonics, The University of Queensland
¶Research Scholar, Centre for Hypersonics, The University of Queensland
‖PhD Candidate, Centre for Hypersonics, The University of Queensland
**Professor, School of Mechanical and Electrical Engineering, The University of Southern Queensland

Subscripts

1	Top layer, calorimeter
2	Substrate
∞	Free-stream condition
l	Calorimeter-substrate interface
s	Surface

I. Introduction

Accurately predicting heating rates is hugely important for the design of hypersonic vehicles, where managing extreme heat loads is required. Thermal protection systems used to shield substructures and cargo from surface heating can constitute a significant proportion of the mass of a vehicle such as an atmospheric entry capsule. Large safety margins are currently used for the design of planetary entry heat shields due to a lack of accurate predictions of heat loads. Improved predictions would reduce risk, increase safety, and lead to increased payloads or reductions in the size of vehicles, all important factors contributing to the success of missions.

Flight testing is expensive, so the majority of hypersonic testing is performed in ground based facilities. Of these ultra-high speed impulse wind tunnels, those capable of producing total enthalpies equivalent to flight and matching binary scaling parameters have tests times of the order 10 µs to 2 ms.[1] Thus, instrumentation used must have sufficiently fast response times to produce useful data. By the nature of the facilities' operation, test flows can be contaminated with particulates and fragments of metallic diaphragm which impact models at high speeds. Once stagnated in front of blunt body models, the flow can become significantly ionised which can interfere with electronics. These problems provide challenges for the accurate measurement of surface heat transfer rates. Thin film heat transfer gauges which are commonly used in low enthalpy testing only survive one shot when mounted on blunt body geometry in high enthalpy facilities.[2]

Promising advances in robust gauges include thermocouples where a surface junction is formed either by mechanical interference[3] or abrasion.[4] However, these gauges may still require re-abrading or re-machining between shots due to damage from the flow. There are also uncertainties associated with the thermal product of coaxial thermocouples[5] of up to 20 % depending on the location of the junctions and changes of up to 30 % at microsecond time-scales.[6] Good electrical grounding, which is difficult to achieve, is necessary to avoid interference from ionised flows.

By using a calorimeter style gauge, a fragile temperature sensing element can be shielded from direct contact with test flows. The short response time required for hypersonic ground testing can be obtained using a thin calorimeter made from a material with a high thermal diffusivity. Palmer[7] used a 25 µm copper calorimeter which could survive 3 to 4 shots in the X2 expansion tube. Diamond has a much higher thermal diffusivity than copper, mainly due to its exceptionally high thermal conductivity which is between 1000 W K/m to 2600 W K/m.[8] The Chemical Vapour Deposition (CVD) process allows synthetic diamond to be grown from a seed crystal with conditions tailored to promote growth of either Single Crystal Diamond (SCD) or Poly-Crystalline Diamond (PCD). The crystalline structure dictates the optical, mechanical, and thermal properties of the diamond. Opaque PCD can be produced by controlling the size of the crystals such that total internal reflection occurs. Additionally, synthetic diamond has a high impact hardness; it is used as a coating on high speed cutting tools.

Initial investigation of the use of CVD diamond as a calorimeter material[9] was undertaken at The University of Oxford by Clark[10] and Vanyai. Further development to the point of a practicable heat transfer gauge is the focus of the current study.

The background behind the DHTG is discussed in Section II with an analysis of how different materials and substrates affect response time and accuracy. The design of the new Diamond Heat Transfer Gauge (DHTG) is presented in Section IV with results from calibration experiments and an analysis of measurement uncertainty Section V. Finally the results from experiments at low and high total enthalpies are presented and discussed in Section VI.

II. Background

A. Calorimeter Analysis

Typical sensor designs for measuring heat flux in high speed transient facilities rely on surface temperature measurements using either Thin Film Heat Transfer Gauges (TFHTG) or thermocouples (TC).[5] By measuring the temperature directly at the surface of a model, the fastest possible response time can be obtained. The drawback of surface measurement is that the sensing element, which is often delicate and subject to interference from the flow, is directly exposed. Sub-surface temperature measurement removes this problem but makes reproducing the surface heat flux more challenging. Directly solving the inverse heat equation for a sub-surface temperature measurement is a well-known ill-posed boundary condition problem[11] and solutions generally involve a least-squares minimisation estimate and are highly sensitive to measurement noise.[12]

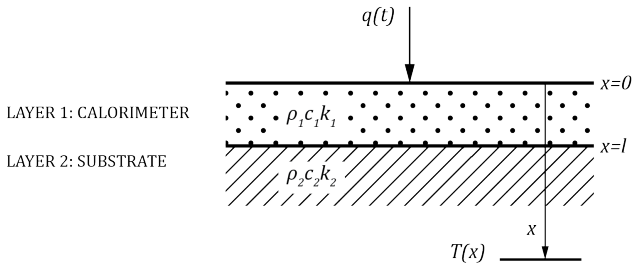

Figure 1: Schematic of a 1D analysis of a calorimeter gauge.

A simple solution, which is accurate under conditions explored in this section, is to model the system as a calorimeter. The net energy into a slab of material (the calorimeter) is equated to the energy needed to raise its average temperature. Figure 1 shows a schematic of a multi-layer system for which the equation for the diffusion of heat can be written:

$$\frac{\partial T_n}{\partial t} = \alpha_n \frac{\partial T_n}{\partial x^2} \tag{1}$$

Where $n = 1, 2$ and represents the layer number. The surface heat flux can be written using the calorimeter equation with temperature dependent properties:

$$\dot{q}_s(t) = \rho_1 c_1 l \frac{d\overline{T}(t)}{dt} + \dot{q}_{loss}(t) \tag{2}$$

Where $\overline{T}$ is the average temperature of the calorimeter, defined as:

$$\overline{T}(t) = \frac{1}{l}\int_0^l T_1(x,t)dx \tag{3}$$

The only loss in the system shown in Figure 1 is conduction into the substrate. If the temperature at $x = l$ is known (T_l), the heat flux lost can be modelled by considering 1D conduction into a semi-infinite substrate:[5]

$$\dot{q}_{loss}(t) = \sqrt{\frac{\rho_2 c_2 k_2}{\pi}}\left[\frac{T_l(t)}{\sqrt{t}} + \int_0^t \frac{T_l(t) - T_l(\tau)}{(t-\tau)^{3/2})}d\tau\right] \tag{4}$$

It is important to note that material and physical properties can have significant temperature dependence which must be accounted for in the analysis presented here.

B. Rear surface temperature measurement

Equation 2 requires measurement of the mean temperature of the calorimeter to reproduce the surface heat flux. For a practical gauge such as is depicted in Figure 2 the mean temperature cannot be measured, so the

key requirement is that the measured temperature gradient can be considered equal to the mean temperature gradient, with respect to time:

$$\frac{dT_{measured}(t)}{dt} = \frac{\overline{T}(t)}{dt} \tag{5}$$

The parameters that affect the validity of Equation 5 are evaluated below over short and long time-scales.

1. *Short term response and rise time*

For the case of a calorimeter with no losses and a step change in heat flux input, the rear surface temperature gradient approaches that of the mean. The time taken for the measured temperature gradient to come within 1 % of the mean is defined as the rise time, τ_{rise}. To produce a gauge which can measure high frequency fluctuations in surface heat flux, the rise time must be minimised. This can be achieved by minimising the thickness of the calorimeter and choosing a material with a high thermal diffusivity. Schultz and Jones[5] give an approximation for the rise time:

$$\tau_{rise} = \frac{l^2}{2\alpha_1} \tag{6}$$

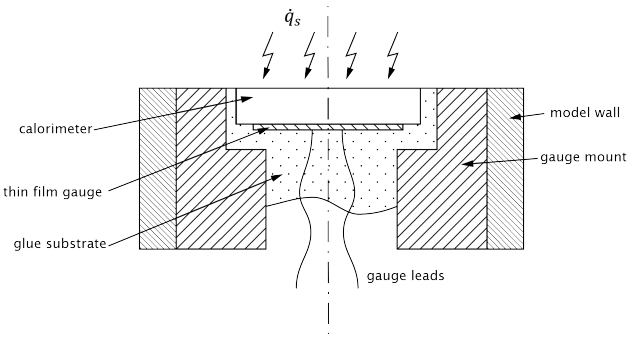

Figure 2: Schematic of the DHTG.

The extraordinarily high thermal conductivity of diamond and the fact it can be manufactured in very thin homogeneous pieces through the Chemical Vapour Deposition (CVD) process makes it stand out as a candidate material for a calorimeter. The thermal properties of different grades of CVD diamond are compared to Copper and Silicon Carbide in Table 1. Using these material properties, the rise time as defined by Equation 6 is plotted in Figure 3 as a function of thickness. For the same thickness of calorimeter, using SCD or transparent PCD instead of copper gives around an order of magnitude reduction in rise time.

Table 1: Thermal properties of synthetic diamond and alternatives

Material Property	Units	SCD	PCD (Transparent)	PCD (Opaque)	SiC	Copper
Density, ρ	$\mathrm{kg\,m^{-3}}$	3514	3514	3514	3100	8960
Heat Capacity, c	$\mathrm{J\,kg^{-1}\,K^{-1}}$	495	495	495	750	385
Conductivity, k	$\mathrm{J\,m^{-1}\,K^{-1}}$	2000	1800	1000	120	380
Diffusivity, α	$\mathrm{m^2\,s^{-1}}\ \times 10^{-6}$	1150	1035	575	52	114
Effusivity, e	$\mathrm{J\,s^{1/2}\,m^{-2}\,K^{-1}}\ \times 10^{3}$	67.0	63.5	47.4	34.7	36.2

2. *Long term response and measurement accuracy*

Losses in the form of conduction into the substrate affect the temperature gradient of the rear surface. The error introduced compared to an ideal insulating case is defined by Equation 7. Temperature gradients from

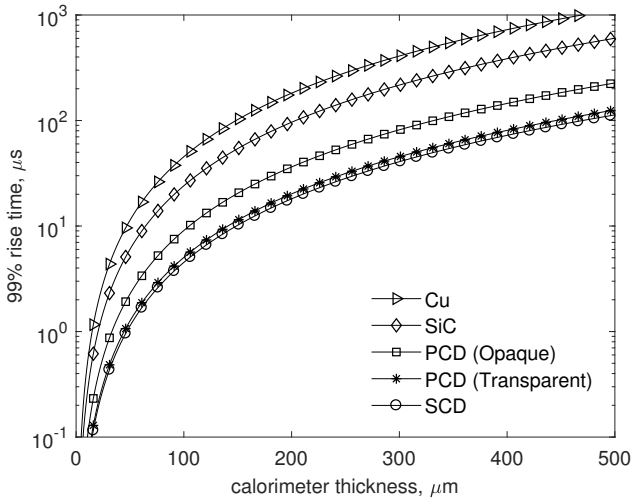

Figure 3: The theoretical response time of an ideal calorimeter based on the 99 % rise time of the rear surface temperature gradient as a function of calorimeter thickness. Plotted for materials shown in Table 1.

a 1D finite difference model of heat diffusion through a 100 µm PCD calorimeter with a range of substrates are shown in Figure 4. The accuracy of the calorimeter assumption is shown to be a function of the ratio of thermal effusivities, defined in Equation 8. For a given calorimeter material, the higher the thermal effusivity of the substrate the less accurate the measured surface heat flux is. The rise time of the rear surface temperature gradient is shown to be independent of substrate material.

$$\text{temperature gradient error} = \frac{\frac{dT_{measured}}{dt} - \frac{d\overline{T}}{dt}}{\frac{d\overline{T}}{dt}} \tag{7}$$

$$\mathrm{a} = \frac{\sqrt{\rho_2 c_2 k_2}}{\sqrt{\rho_1 c_1 k_1}} \tag{8}$$

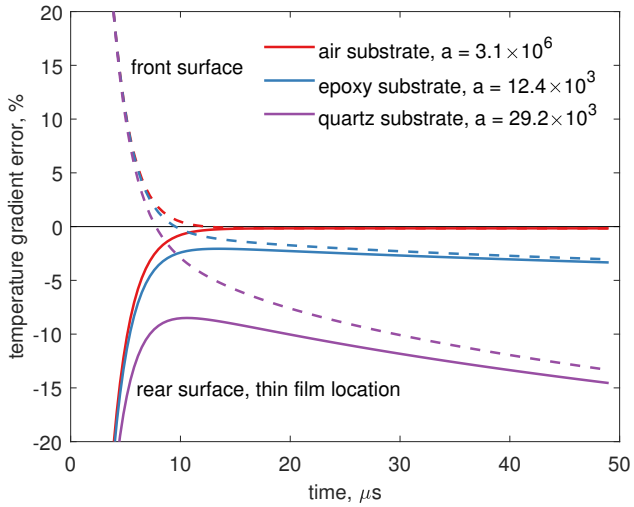

Figure 4: Front and rear surface temperature gradient error, as defined by Equation 7, from a 1D finite difference model of a 100 µm transparent PCD diamond calorimeter with three possible substrates. Surface heat flux 10 MW m^{-2}.

III. Thin Film Resistance Temperature Device (Thin Film RTD)

The heat transfer gauge developed uses a platinum thin-film RTD to measure temperature rise of the rear surface of the calorimeter. A thin film RTD consists of a track of conductive material, normally Platinum or Nickel, deposited on a substrate with leads connected to pads at either end. The width and thickness of the track is limited such that the resistance between the pads is generally 30 Ω to 80 Ω.

For pure metals, resistance increases as temperature increases, so a change in temperature can be measured through a change in resistance. The resistance of an element can be written as a function of temperature and the parameters α_R and R_0 which are the temperature coefficient of resistance and the resistance at 0 °C. These values can obtained by a calibration method described in Section V.A.

$$R = R_0(1 + \alpha_R \Delta T) \tag{9}$$

For measurements at high frequencies, a constant current across the resistive element is applied, and the change in resistance can be measured through a change in voltage. Schultz and Jones[5] define the change in temperature as:

$$\Delta T = \frac{I_0 \Delta R}{\alpha_R I_0 R} = \frac{\Delta V}{V_0 \alpha_R} \tag{10}$$

The recorded voltage transformed into temperature can then be used to calculate the surface heat flux using Equation 2.

It can be seen from Equation 10 that the sensitivity of a thin film depends on the voltage across it. The sensitivity therefore is dependent on the supply current of the amplifier used and the resistance of the gauge. Using the University of Queensland heat transfer gauge amplifiers with nominal values, R =50 Ω and $\alpha_R = 2.5\times10^{-3}$, the sensitivity is 1770 µV/°C.

IV. Gauge Design

Based on the theoretical response described in the previous sections, a range of gauges with different calorimeter thicknesses and materials were made to provide a range of response times, as shown in Table 2. This range of thicknesses also allowed the influence of calorimeter thickness on robustness to be investigated. It was theorised that gauges with thicker diamond layers would be more robust and so more suited to stagnation point or high angle of attack testing in hypersonic facilities. Thinner diamond layers have faster response times but were presumed to be more delicate and so more suited to low angles of attack or facilities without a lot of particles in the flow.

Table 2: Theoretical rise times of current types of DHTG calculated using Equation 6. 75 µm gauges have not yet been tested.

Nominal thickness, µm	Material	95 % rise time, µs	99 % rise time, µs	DHTG Numbers
75	SCD	1.88	2.64	planned
150	PCD	8.37	11.7	1 to 5, 16, 17
200	PCD (Opaque)	33.5	47	6 to 10
300	PCD (Transparent)	26.7	37.3	11 to 15

The sensor is defined as the assembly of the diamond calorimeter and the platinum thin film gauge as shown in Figure 5a. A 0.15 mm wide platinum track is sputtered onto a disk of CVD diamond with leads bonded to gold pads. The length of the platinum track is fixed, and the resistance of between the pads is specified to be between 45 Ω to 55 Ω. The sputtered depth of the track is increased until the desired resistance is reached.

The gauge is defined as the completed assembly of the sensor in its housing. A cross-section view of the gauge is shown in Figure 5b. The sensor is fixed with high temperature resistant epoxy into a high tensile steel housing. The recess in which the sensor sits is larger than the diameter of the diamond disk to allow a

layer of epoxy to thermally insulate the two pieces. A condition for the minimum depth of a substrate such that it acts as an semi-infinite medium over a short test time is given by Schultz and Jones[5] as:

$$x = 4\sqrt{\alpha_2 t} \tag{11}$$

Where x is the depth and t is the test time. The minimum depth of epoxy, such that it behaves as a semi-infinite substrate over a nominal 500 µs test time can therefore be calculated as 0.063 mm. To provide a margin of error, an epoxy depth of at least 0.5 mm was specified.

The design of the gauge body went through multiple iterations which are shown in Figure 6. Each iteration improved the reliability with which the gauges could be assembled and the reliability of the gauges while in use. This led to the standard gauge design shown in Figure 6b which was used for tunnel testing in the X2 (see SectionVI). Figure 6c shows a newer version, slightly modified for use with the backing nut also pictured.

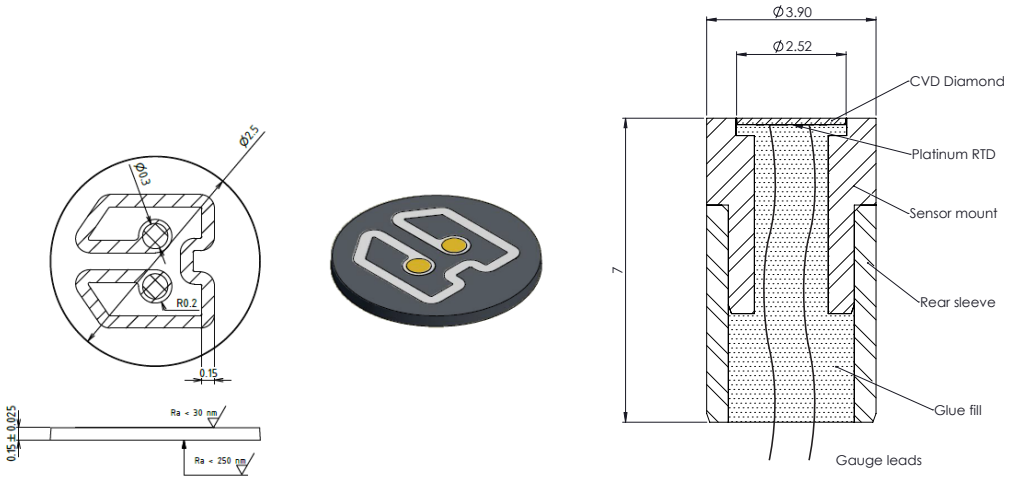

(a) Drawing of the sensor: a 2.5 mm by 150 µm thick CVD diamond disk with a platinum thin film RTD on one side and gold pads to bond leads to.

(b) Section view drawing of a DHTG.

Figure 5: Drawings of the sensor and DHTG.

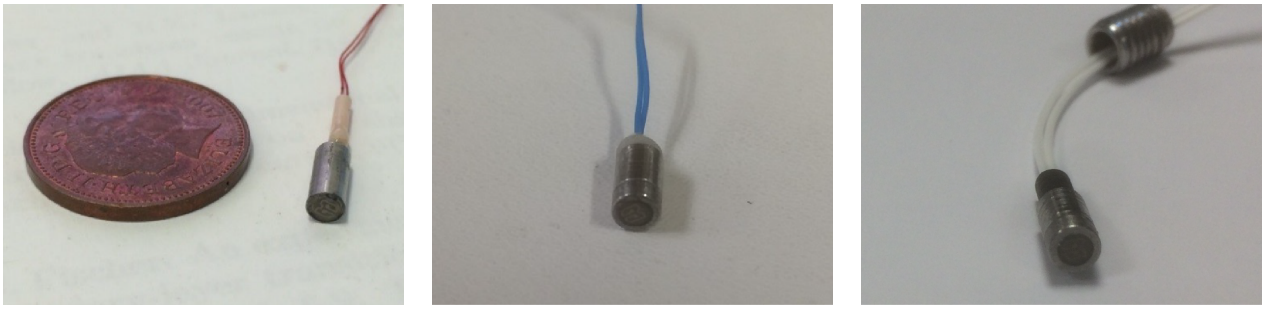

(a) Version 1

(b) Version 2

(c) Version 3

Figure 6: Photos of the first three versions of the DHTG with a 1 pence coin for scale. Version 3 is installed in a model using a backing nut.

V. Calibration procedures and sources of measurement uncertainty

This section describes procedures used to calibrate each platinum thin film element and to determine and minimise the measurement uncertainty.

A. Static calibration

Static calibration of the platinum thin film in each gauge is required to find the temperature coefficient of resistance (α_R) which is used in Equation 10 to calculate the change in temperature of the thin film. The calibration procedure described here was developed by Collins.[13]

A batch of gauges are submerged in a waterproof bag into a bath of water. The bath temperature is stepped at least four times through a temperature range of 15 °C to 75 °C in increments of 15 °C. The temperature of the water bath and the gauge bodies are monitored with thermocouples. The water bath temperature is held at each step until the measured temperatures converge to within a specified tolerance, usually 0.2 °C. Once convergence has been achieved and held for 10 minutes the system is assumed to be isothermal and the resistance across each sensor is recorded.

A linear regression is performed on the recorded resistance and temperature data to find dR/dT, and R_0. Equation 12 is then used to find α_R. The DHTGs calibrated using this method all show highly linear characteristics, with $\Delta\alpha_R < 1\%$ at 95 % confidence.

$$\alpha_R = \frac{dR/dT}{R_0} \tag{12}$$

B. Sources of uncertainty

Uncertainty from each step in the calculation of surface heat flux using a DHTG is quantified and combined to give an overall measurement uncertainty. Some of the uncertainties are dependent on temperature, in which case a nominal rise from 20 °C to 120 °C is used. This is representative of a 200 MW/m^2 incident surface heat flux applied for 200 µs to a 200 µm thick PCD calorimeter. The sources of uncertainty are:

1. The calibration of the thin film element which determines the value of α_R. An uncertainty of less than 1 % is arises from fitting the regression to the recorded data. The error in measuring the water bath temperature and the resistance is considered negligible.

2. The thickness of the calorimeter. A sample of each nominal thickness of diamond was measured. The mean of the measurements is given below, with the tolerance at 95 % confidence:

   - Nominally 300 µm: 324 µm ±1.4 %
   - Nominally 200 µm: 216 µm ±2.1 %
   - Nominally 150 µm: 154 µm ±10.2 %
   - Nominally 75 µm: 75 µm ±26 % (not measured, manufacturer tolerance)

3. The specific heat capacity of the calorimeter. Interpolated temperature dependent data from Kaye[8] and[14] was used. Differences in heat capacity due to the different micro-structural crystal length scales of PCD and SCD have been shown to be insignificant,[15] so the same values were used for all types. The uncertainty of these measurements is not stated in the source. The standard laser-flash method to determine thermal properties has a typical error of 10 %,[16] which is used in this analysis.

4. The density of the calorimeter. Data obtained from Kaye,[8] where an uncertainty of 10^{-3} % is stated. Density has negligible temperature dependence over the 20 °C to 120 °C range.

5. Thermal expansion changing the dimensions of the calorimeter. Radial and axial dimensions of the calorimeter have negligible change over a 20 °C to 120 °C temperature rise: less than 0.05 %.

6. Conduction losses to the substrate. Heat flux lost through combined axial and radial conduction with an epoxy substrate has been estimated to be 2.25 % of the surface incident heat flux and is accounted for in the calculation of surface heat flux.

The listed sources of uncertainty are combined using the Root-Sum-Square method described by Moffat[17] to give the overall measurement uncertainties for each thickness of calorimeter shown in Table 3. The greatest contribution to the measurement uncertainty for the 200 µm to 300 µm pieces is the uncertainty in the specific heat capacity of diamond. For the thinner diamond pieces the uncertainty in the thickness of the diamond layer becomes dominant. Planned measurements of diamond pieces on an individual basis will reduce this in the future.

Table 3: Surface heat flux measurement uncertainty for DHTGs of different thicknesses

Nominal calorimeter thickness, µm	300	200	150	75
RSS uncertainty in q_s, %	10.1	10.3	14.3	27.9

VI. Experimental Testing

In this section experiments conducted to investigate the performance and robustness of the gauge are described. Three main experimental aims were defined:

1. To validate the measured heat flux from DHTGs against existing measurement techniques,
2. To quantify the robustness of the DHTGs in high enthalpy facilities, including the effect of different thicknesses diamond layers,
3. To compare experimentally determined rise times to theoretical rise times.

Preliminary tests were performed in a low enthalpy shock tube at the University of Oxford which uses Mylar diaphragms and has a free-stream flow velocity of less than 1 km/s. Good agreement in measured heat flux was shown between a DHTG and a platinum thin film heat transfer gauge. The results gave confidence in continuing the development of the DHTG and to move to test the robustness of the gauges in higher enthalpy facilities.

The subsequent testing described in this section took place in the X2 expansion tube facility at the University of Queensland, Australia. The operation of X2 involves bursting a steel diaphragm; the flow contains diaphragm particles which impact the model and tested the robustness of the new gauges. Surface abraded coaxial thermocouples developed by David Buttsworth[4] were tested alongside the DHTGs.

This section describes the flow conditions which were used for testing, the model in which heat transfer gauges were mounted and the results of the campaign including an analysis of the robustness of the gauges.

A. The X2 expansion tube facility

The X2 Expansion Tube is a free-piston driven impulse flow facility which can produce scaled test flow conditions for atmospheric entry into most planets in our solar system.[18] X2 has multiple modes of operation, but for the purposes of this test campaign the tunnel was operated as an expansion tube with a single driver tube and a diverging nozzle at the test section entrance. Details of the X2 expansion tube can be found in Gildfind et al.[19] An overview of expansion tubes in general can be found in Morgan.[20]

B. Conditions

The nominal test section flow conditions tested at are shown in Table 4. Conditions A to D sweep through a velocity range at roughly constant density. Condition E returns to a mid-range velocity but with an order of magnitude higher density. This set of flow conditions allowed the robustness and response of DHTGs to be evaluated across a range of flow velocities and heat flux inputs. Air was used as the test gas for all conditions.

Test section flow conditions were calculated for each shot from the fill conditions and measured acceleration tube shock speeds using a UQ in-house simulation code named PITOT.[18]

Table 4: Details of the conditions used in the X2 campaign including nominal test-section free-stream flow properties and a description of what the condition was originally designed for. All conditions used air as the test gas.

Condition	U_∞ (km/s)	ρ_∞ (kg/m^3)	M_∞	Leading edge	Shot Qty.	Shot Numbers	Description
A	7	1×10^{-3}	10.0	Sharp	3	x2s3482 - x2s3484	1/52 scaled IXV entry[21]
				Blunt	3	x2s3504 - x2s3506	
B	9	1×10^{-3}	10.4	Sharp	3	x2s3490 - x2s3491	Hot wall TPS testing[22]
C	10	2×10^{-3}	12.2	Sharp	3	x2s3492 - x2s3494	1/5 scaled Hayabusa entry[23]
D	11	1×10^{-3}	10.3	Sharp	4	x2s3495 - x2s3498	VUV radiation study[24]
E	9	10×10^{-3}	5.2	Blunt	4	x2s3507 - x2s3510	1/42.1 scaled Apollo entry

C. Model

A schematic of the model designed and built for testing in X2 can be seen in Figure 7 and photos are shown in Figure 8. The model can either be fitted with a sharp leading edge or a blunt leading edge with a 21.65 mm radius of curvature. When fitted with the sharp leading edge the model was mounted such that one side was at 0° AOA and the other side at 22.5° AOA. This allowed data to be gathered from two angles of attack for each shot. When fitted with the blunt leading edge the underside was set to 45° AOA.

Twenty gauges total, arranged in two parallel lines of five holes on each side of the model allowed comparison between different types of heat transfer gauge at the same axial location. When the blunt leading edge was installed, two additional gauges were mounted on the stagnation point. Leads from all gauges ran out of the model through a hollow sting, to amplifiers, and then to a data acquisition system.

A pressure transducer (PCB 113B) was mounted on the angled side of the model to allow the conditions to be compared and the test time to be determined.

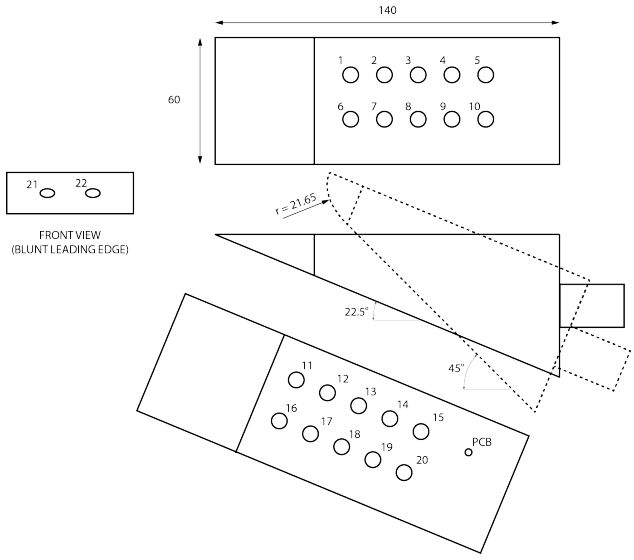

Figure 7: Schematic of the model used for testing in X2 with hole numbers labelled. All dimensions in mm.

D. Processing of experimental data

Recorded voltages from DHTGs and TCs were used to calculate surface heat flux. Equation 2 was used to calculate the heat flux for the DHTGs. Thermal properties of the calorimeter were updated at each time-step using data from Kaye.[8] The impulse response method developed by Oldfield[25] was used to calculate the

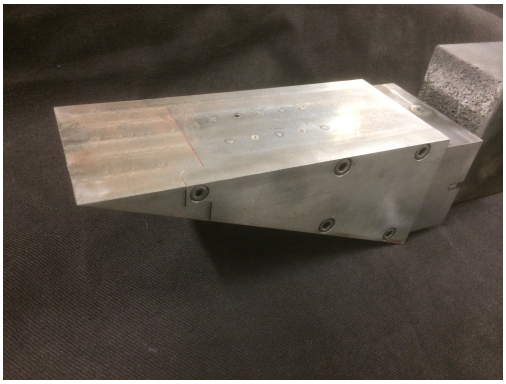

(a) The model with sharp leading edge installed.

(b) The model in the test section with the blunt leading edge installed.

Figure 8: Photos of the model which heat transfer gauges were mounted in for experimental testing in X2.

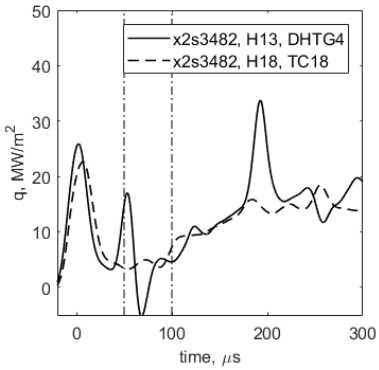

(a) Condition A, sharp leading edge

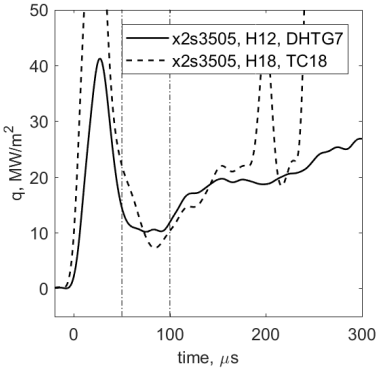

(b) Condition A, blunt leading edge

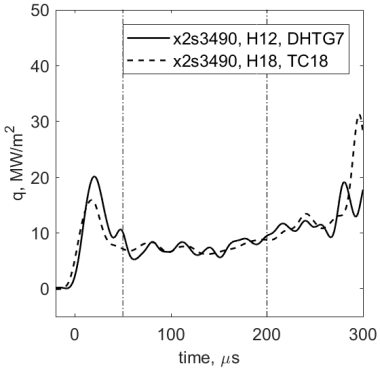

(c) Condition B

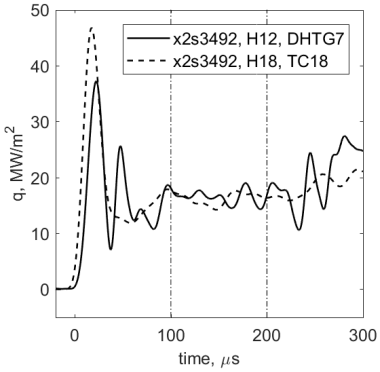

(d) Condition C

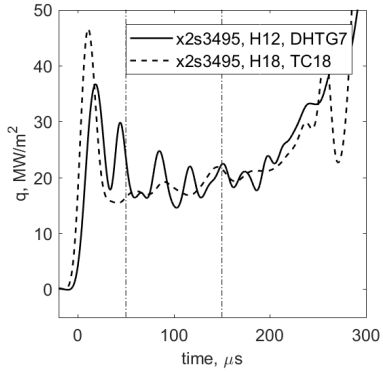

(e) Condition D

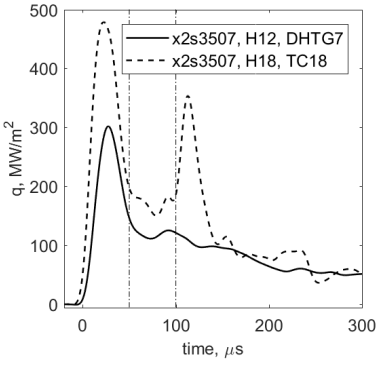

(f) Condition E

Figure 9: Heat flux from DHTG13 in hole 11 for condition A with the sharp leading edge and DHTG7 in hole 12 for all other shots of the X2 campaign. Test times are between the vertical dashed lines. Data has been filtered using a moving average filter.

heat flux for the thermocouples. This method models heat transfer into the gauge as conduction into a homogeneous semi-infinite substrate. The method requires a single value of the thermal product which must be an average of the two thermocouple metals, Constantan and Chromel. The thermal product was taken to be $10\,500\,\mathrm{J\,s^{1/2}\,m^{-2}\,K^{-1}}$, as per Mohammed.[26]

E. Surface heat transfer results

The measured surface heat flux from a DHTG and a TC are compared in Figure 9 for one shot at each flow condition (condition details are shown in Table 4). The signal from DHTG7 in hole 12 and TC18 in hole 18 are used for all conditions apart from condition A with the sharp leading edge installed. For shots at this condition DHTG7 had a faulty electrical connection and so DHTG4 is used. Good agreement is clearly shown between the two types of gauge across a wide range of flow enthalpies.

Heat flux measurements from the three shots at condition E, the highest enthalpy condition, are presented in Figure 10. The locations of the gauges are labelled on a section view of the model. On the stagnation point the heat flux from two nominally identical DHTGs is compared. At each axial location on the wedge, the measured heat flux from a DHTG and a TC is compared. Data from both types of gauge has been filtered using a low-pass filter with a cut-off frequency of 200 kHz to improve legibility. The test time for each case is indicated by vertical dashed lines on each plot.

Overall, the signal from the thermocouples is more erratic than the DHTGs. The first theory for why this may be, is that the fluctuations shown are real flow features which the thermocouples can resolve because their response time is faster than the DHTGs.

A second theory is that it could be caused by interference to the exposed junction from ionised flow: the stagnation point post-shock temperature at chemical equilibrium is estimated to be 11 000 K. This is above the 9000 K threshold at which ionisation of air becomes a significant consideration.[27] Although the thermocouples were fitted with a grounding wire attached to their body to alleviate this issue, true grounding is difficult to achieve.

A third theory is that the fluctuations are caused by increased electrical interference picked up by cabling between the gauge and the amplifier. Both types of gauges used similar lengths and types of cabling but the sensitivity of the thermocouples which is 63 µV/°C compared to 1770 µV/°C for the DHTGs means that the signal to noise ratio for a similar temperature rise is significantly worse.

The results presented in Figure 10 are now discussed for each axial location in turn, starting at the stagnation point:

1. *Axial location 1: DHTG15 and DHTG11*

An empirical correlation developed by Sutton and Graves[28] for stagnation point convective heat flux shown in Equation 13 is plotted with the measured stagnation heat fluxes in Figure 10. For the shots presented in this figure, DHTG11 had no response and was assumed to be broken. The correlation is given in the form presented by Brandis and Johnson[29] for Earth entry. Brandis and Johnson's more accurate updated convective heat flux correlation was not used because the free-stream density for Condition E is outside of the stated limits.

$$\dot{q}_s = 0.188\sqrt{\frac{\rho}{R}}\left(\frac{V}{1000}\right)^3 \tag{13}$$

The heat flux is measured in $\mathrm{MW/m^2}$. R is the nose radius in metres and V is the velocity in m/s.

The correlation is only valid over the marked test time. During this period the DHTGs predict, on average, a higher heat flux than the correlation by around 20 %. When the measurement uncertainty of the gauges and the error in the correlation are taken into account, this is can be considered good agreement.

2. *Axial location 2: DHTG13 and TC16*

DHTG13 measured a lower heat flux than both the stagnation point gauge and the downstream gauges over all three shots. The largest difference is during flow establishment at 50 µs to 100 µs where the measured peak is around half that which the downstream DHTGs measured. During the test time the difference is reduced, but still apparent.

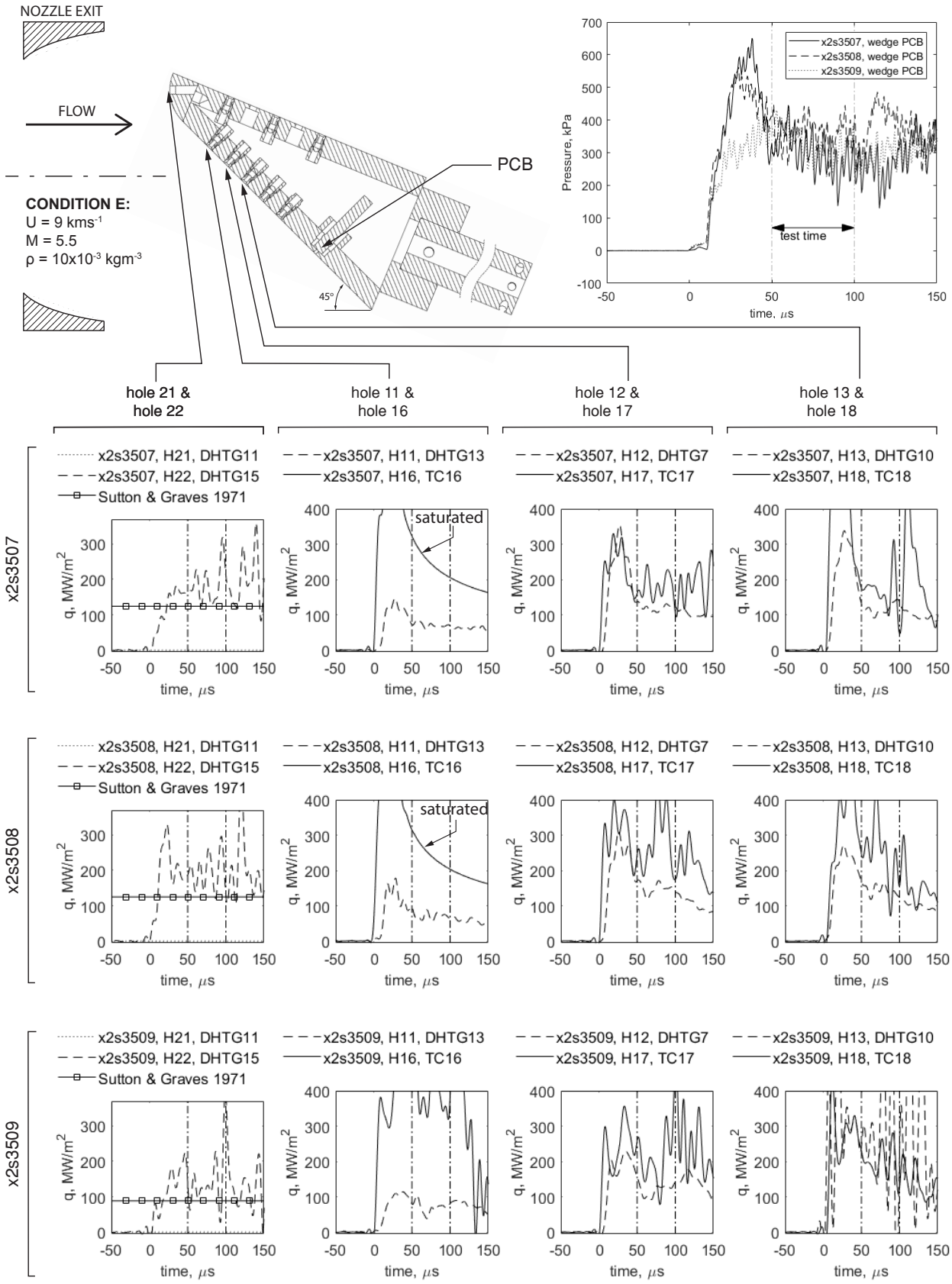

Figure 10: Condition E: measured heat flux from DHTGs and thermocouples. Vertical dashed lines indicate the start and the end of the test time. The pressure recorded from the PCB mounted downstream on the wedge surface of the model shown in the top right. The decaying response shown for TC16 in Hole 16 for shots x2s3507 and x2s3508 is due to the signal saturating the amplifier, and is not a real heat flux.

The thermocouple signal saturated the amplifier for the first two shots, producing the non-physical decaying response shown. For the third shot it measured the highest average heat flux of any gauge over the shots presented.

3. *Axial location 3: DHTG11 and TC17*

The gauges at this location show good agreement, with the thermocouple in general predicting a slightly higher heat flux than the DHTG. The gauges at this axial location and furthest downstream location measure a heat flux over the useful test time which is higher than what is measured by the upstream gauges, including the stagnation point. This suggests that laminar to turbulent transition of the boundary layer may have occurred. Further investigation with more repeat shots at the same flow condition is necessary to instigate this theory.

4. *Axial location 4: DHTG10 and TC18*

DHTG11 in hole 13 shows a significant change in response during the third shot (x2s3509) compared to the previous two shots. The change is due to damage to the gauge. How damage to the calorimeter and the thin film affects the accuracy of measured heat flux is discussed further in Section VI.F.3.

F. Robustness of the gauges

Between each shot in X2 a photo of the surface of each gauge was taken and the resistance across the sensor was recorded with a multimeter. The photos of the gauges in Figure 11 show evidence the extreme environment which the gauges must survive. Craters from diaphragm fragment impacts can be seen on the surface of the high tensile steel model, can be seen in all photos apart from Figure 11a.

1. *TC robustness*

All but one of the thermocouples used were still functional at the end of the campaign. The abrasive nature of the expansion tube flow at high enthalpies is actually beneficial: new surface junctions are created by impacts. This is not to say that the thermocouples were perfect throughout the campaign, in fact, for many shots the signal from the thermocouples was too erratic to be of use. The problem was not with the thermocouples themselves, but rather their extreme sensitivity to electrical noise. Small movements of cabling which are unavoidable in the experimental environment sometimes rendered signals unusable.

2. *DHTG robustness*

The survival rate for DHTGs on the flat plate side of the model was 100 %. Of the ten DHTGs that were mounted at an angle of attack, four ended the campaign without any sign of damage, having been used for 17 shots on average. Four gauges were destroyed, surviving 1.75 shots on average. Two gauges showed a change in resistance across the thin film but were still functional, this is discussed further in Section VI.F.3.

Photographs of the surface of DHTG15 are shown before and after it broke in Figure 11a and Figure 11b respectively. The surface of the diamond is pristine before the shot, and a crater from a diaphragm fragment impact can be seen after. The impact severed the continuity of the platinum film on the rear side of the diamond layer. Judging by the photographs, DHTG7 and DHTG11 would appear to have been damaged more than DHTG15, yet were still functioning after many more shots. Either the gauges that broke quickly were hit in an unfortunate location by a diaphragm fragment or some gauges had manufacturing defects making them more prone to break than others. The sample it far too small to propose a link between thickness of diamond and robustness.

3. *Functional DHTGs with a resistance change*

Figure 12 shows the resistance measured across the leads of the DHTGs in use for shot x2s3496 to x2s3510. DHTG10 and DHTG11 show a significant change over a number of shots. DHTG15 broke during shot x2s3504. The gauges were re-calibrated after the campaign, using the same method and apparatus as before. Table 5 shows the percentage change in calibrated values and the error which using the original calibration

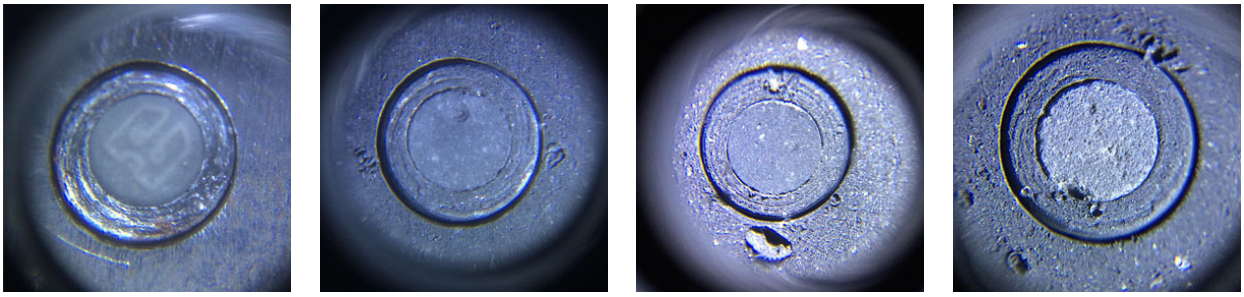

(a) DHTG15, 0 shots, working (b) DHTG15, 1 shot, broken (c) DHTG7, 25 shots, working (d) DHTG11, 9 shots, functional but with a change in electrical resistance

Figure 11: Microscope photos of the surface of some DHTGs.

introduces to the measured heat flux. A strong link between resistance change at ambient conditions and calibrated values is clear.

The ideal result of this analysis would be a relationship between ambient resistance change to the introduced error in measured heat flux. This would allow a simple measurement of resistance between shots in a future campaign to dictate whether a gauge is too damaged to continue being used because the measurement error is too high. The sample size of the data at hand is small: only two gauges showed a significant resistance change. A tentative conclusion can be drawn that a change in resistance at ambient conditions of over $1\,\Omega$ means that the thin film has been damaged and there may be significant measurement error.

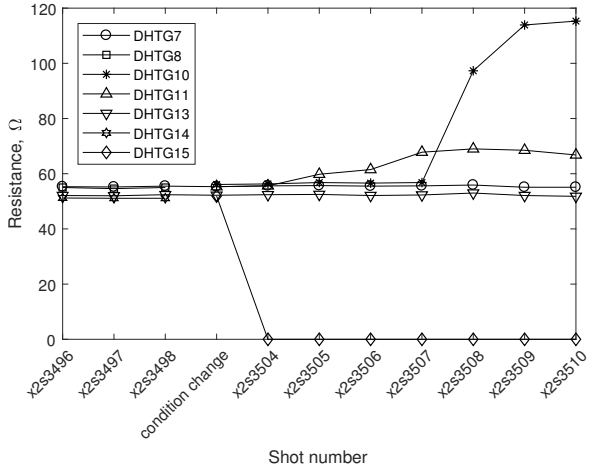

Figure 12: Measured resistance across DHTGs. The measurement was taken after the labelled shot number across the leads at the inputs to the amplifier, meaning lead resistance is included

G. Experimental rise time

An estimate of rise time can be defined as the time from when a shock first arrives at a gauge and initiates flow to when the heat flux measurement reaches steady state or a local maximum. This is not a rigorous calculation of rise time, since the measurement is not in response to a step change in input, but it gives an approximation.

As an example, how the rise time was calculated for DHTG7 for shot x2s3505 in X2 is shown in Figure 13. The shock arrives at $t = -3.7\,\mu s$ because $t = 0$ is taken as the arrival of the shock at the PCB, which is downstream of the heat flux gauges. The pressure gauge was mounted in a recessed hole, the inset plot shows a gradual rise from shock arrival which is due to the filling time of the recess. A similar method was used with data from shots performed in the low enthalpy shock tube which is briefly described at the beginning

Table 5: Change in results from static calibration after testing in X2. Error in heat flux measurement is calculated as per Section V.B with all other parameters at their nominal values. DHTG10 had a resistance of over 200 Ω when measured after the calibration had been completed, making it effectively open circuit for the calibration process.

DHTG No.	$\Delta R_{ambient}$, Ω	ΔR_0, %	$\Delta\alpha_R$, %	q_s error, %
5	1.4	-5.07	6.09	11.8
7	0.1	-0.18	0.21	0.4
8	0.7	0.25	0.12	0.5
10	59.2	unknown	unknown	unknown
11	11.5	-29.50	-26.61	64.7
12	0	0.29	0.03	0.6
14	0	-0.21	0.46	0.6

of this section.

The experimentally estimated rise time shown in Table 6 is the average across all shots which each thickness of calorimeter was used for. The experimentally estimated rise time is shown to be slightly lower than the theoretical 95 % rise time, but agrees well considering the lack of well defined step input.

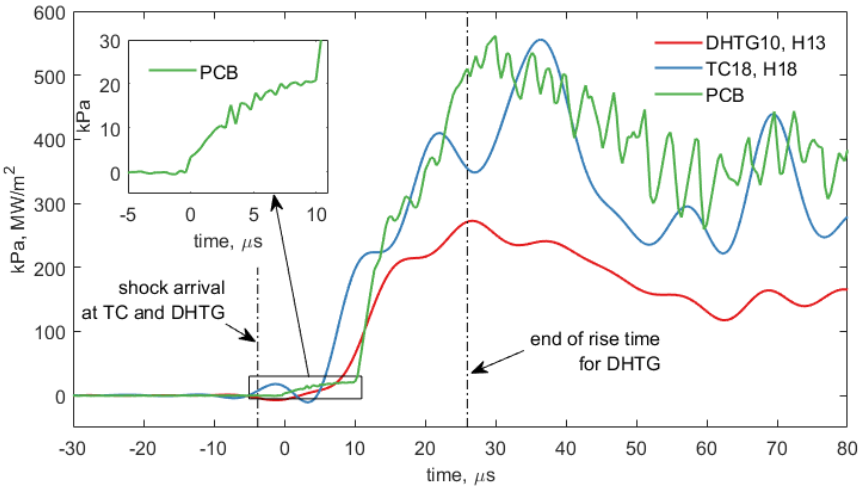

Figure 13: A demonstration of how the experimental response time was calculated. The shock arrives at the heat transfer gauges at $t = -3.7$ µs and the DHTG takes around 30 µs to rise. The inset plot shows the recorded pressure on a smaller time-scale. Shot x2s3508.

Table 6: Gauge rise times for each thickness of calorimeter estimated from experimental data.

Thickness, µm	Theoretical 95 % τ_{rise}, µs	Experimental τ_{rise}, µs	Testing Source
150	8.37	7.1	Small shock tube
200	33.5	26.7	X2
300	26.7	28.0	X2

VII. Conclusion

A new calorimeter-based heat transfer gauge has been designed, fabricated and tested. The DHTG is shown to be a viable alternative to surface abraded coaxial thermocouples for measuring surface heat fluxes in high enthalpy wind tunnels. Multiple gauges with calorimeters made from CVD diamond survived more than 7 shots at the most severe conditions in the X2 expansion tube facility. Damage to gauges which changes the resistance of the platinum thin film by more than 1 Ω have been shown to introduce significant error to the measured surface heat flux. Further testing of the DHTG will be conducted in the T6 Stalker Tunnel[30] using a similar model to asses robustness in a different type of high enthalpy facility.

The measurement uncertainty of the DHTG has been quantified. The overall uncertainty compares favourably to that of coaxial thermocouples. The largest source of uncertainty with the current gauges is the thickness of the CVD diamond layers. Future work will involve accurate measurement of individual CVD diamond pieces to reduce measurement uncertainty for future batches of gauges. Additionally, an accurate method for experimentally measuring the rise time and amplitude-frequency response of gauges is planned, using a radiation based source of heat flux.

Acknowledgements

Thanks to Trevor Godfrey and Gregory King for their extremely delicate and patient work assembling the DHTGs. Thanks to James Carter for machining the model used in X2 and to all the X2 operators who helped run the campaign.

Thanks to Nathan Stern who fabricated the coaxial thermocouples used in X2 and to Byrenn Birch for his initial performance testing of the thermocouples.

References

[1]Stalker, R. J., "Modern Developments in Hypersonic Wind Tunnels," *Aeronautical Journal*, Vol. 110, No. 1103, 2006, pp. 21–40.

[2]Flaherty, W. and Austin, J., "Comparative surface heat transfer measurements in hypervelocity flow," *Journal of Thermophysics and Heat Transfer*, Vol. 25, No. 1, 2011, pp. 180–183.

[3]Sanderson, S. R. and Sturtevant, B., "Transient heat flux measurement using a surface junction thermocouple," *Review of Scientific Instruments*, Vol. 73, No. 7, 2002, pp. 2781.

[4]Buttsworth, D. R., Stevens, R., and Stone, C. R., "Eroding ribbon thermocouples: impulse response and transient heat flux analysis," *Measurement Science and Technology*, Vol. 16, No. 7, 2005, pp. 1487.

[5]Schultz, D. L. and Jones, T., "Heat-Transfer Measurements in Short-Duration Hypersonic Facilities." Tech. rep., DTIC Document, 1973.

[6]Buttsworth, D. R., "Assessment of effective thermal product of surface junction thermocouples on millisecond and microsecond time scales," *Experimental Thermal and Fluid Science*, Vol. 25, No. 6, 2001, pp. 409–420.

[7]Palmer, R., Morgan, R., Palmer, R., and Morgan, R., "Stagnation point heat transfer in superorbital expansion tubes," *35th Aerospace Sciences Meeting and Exhibit*, 1997, p. 280.

[8]Kaye, G., Laby, T., Noyes, J., et al., *Tables of Physical and Chemical Constants, 1995*, New York: Longman Scientific and Technical, 2008.

[9]Holden, M., Personal Communication.

[10]Clark, T., *The Development of a Diamond-Shielded Heat Transfer Gauge for Hypersonic Test Facilities*, Master's thesis, University of Queensland, 2015.

[11]Beck, J. V., Blackwell, B., and Clair Jr, C. R. S., *Inverse heat conduction: Ill-posed problems*, James Beck, 1985.

[12]Ozisik, M. N., *Inverse heat transfer: fundamentals and applications*, CRC Press, 2000.

[13]Collins, M., Chana, K., and Povey, T., "New technique for the fabrication of miniature thin film heat flux gauges," *Measurement Science and Technology*, Vol. 26, No. 2, 2015, pp. 025303.

[14]Barin, I., "Thermochemical Data of Pure Substances,(1989)," *VCH Verlagsgesellshaft*, 1885.

[15]Moelle, C., Werner, M., SzuÈcs, F., Wittorf, D., Sellschopp, M., Von Borany, J., Fecht, H.-J., and Johnston, C., "Specific heat of single-, poly-and nanocrystalline diamond," *Diamond and related materials*, Vol. 7, No. 2-5, 1998, pp. 499–503.

[16]Baba, T. and Ono, A., "Improvement of the laser flash method to reduce uncertainty in thermal diffusivity measurements," *Measurement Science and Technology*, Vol. 12, No. 12, 2001, pp. 2046.

[17]Moffat, R. J., "Describing the uncertainties in experimental results," *Experimental thermal and fluid science*, Vol. 1, No. 1, 1988, pp. 3–17.

[18]James, C., Gildfind, D., Morgan, R. G., Jacobs, P. A., and Zander, F., "Designing and simulating high enthalpy expansion tube conditions," *APISAT 2013: 2013 Asia-Pacific International Symposium on Aerospace Technology*, Japan Society for Aeronautical and Space Sciences, 2013, pp. 1–10.

[19]Gildfind, D. E., Morgan, R. G., and Jacobs, P. A., "Expansion tubes in Australia," *Experimental Methods of Shock Wave Research*, Springer, 2016, pp. 399–431.

[20]Morgan, R., "Free piston driven expansion tubes," 2001, pp. 603–622.

[21]Vella, S., *Expansion Tunnel Heat Transfer Measurements of the ESA-IXV Re-entry Vehicle*, B.E. Honours thesis, The University of Queensland, 2016.

[22]Zander, F., Morgan, R., Sheikh, U., Buttsworth, D., and Teakle, P., "Hot-wall reentry testing in hypersonic impulse facilities," *AIAA journal*, Vol. 51, No. 2, 2013, pp. 476–484.

[23]Fahy, E., Buttsworth, D., Gollan, R., Jacobs, P., and Morgan, R. G., "Experimental and Computational Fluid Dynamics Studies of Superorbital Earth Re-entry," *46th AIAA Thermophysics Conference*, 2016, p. 3532.

[24]Sheikh, U. A., Morgan, R. G., and McIntyre, T. J., "Vacuum Ultraviolet Spectral Measurements for Superorbital Earth Entry in X2 Expansion Tube," *Aiaa Journal*, Vol. 53, No. 12, 2015, pp. 3589–3602.

[25]Oldfield, M. L. G., "Impulse Response Processing of Transient Heat Transfer Gauge Signals," *Journal of Turbomachinery*, Vol. 130, 2008.

[26]Mohammed, H., Salleh, H., Yusoff, M., and Campo, A., "Thermal product of type-E fast response temperature sensors," *Journal of Thermal Science*, Vol. 19, No. 4, 2010, pp. 364–371.

[27]Anderson, J. D., *Hypersonic and high temperature gas dynamics*, Aiaa, 2000.

[28]Sutton, K. and Graves Jr, R. A., "A general stagnation-point convective heating equation for arbitrary gas mixtures," Tech. Rep. TR R-376, NASA, 1971.

[29]Brandis, A. M. and Johnston, C. O., "Characterization of stagnation-point heat flux for earth entry," *45th AIAA Plasmadynamics and Lasers Conference*, 2014, p. 2374.

[30]McGilvray, M., Doherty, L. J., Morgan, R. G., Gildfind, D., Jacobs, P., and Ireland, P., "T6: The Oxford University Stalker Tunnel," *20th AIAA International Space Planes and Hypersonic Systems and Technologies Conference*, 2015, p. 3545.